

Spin relaxation in n -type GaAs quantum wells from a fully microscopic approach

J. Zhou,^{1,2} J. L. Cheng,² and M. W. Wu^{1,2,*}

¹Hefei National Laboratory for Physical Sciences at Microscale,

University of Science and Technology of China, Hefei, Anhui, 230026, China

²Department of Physics, University of Science and Technology of China, Hefei, Anhui, 230026, China[†]

(Dated: September 30, 2018)

We perform a full microscopic investigation on the spin relaxation in n -type (001) GaAs quantum wells with $\text{Al}_{0.4}\text{Ga}_{0.6}\text{As}$ barrier due to the D'yakonov-perel' mechanism from nearly 20 K to the room temperature by constructing and numerically solving the kinetic spin Bloch equations. We consider all the relevant scattering such as the electron-acoustic-phonon, the electron-longitudinal-optical-phonon, the electron-nonmagnetic-impurity and the electron-electron Coulomb scattering to the spin relaxation. The spin relaxation times calculated from our theory with a fitting spin splitting parameter are in good agreement with the experimental data by Ohno *et al.* [Physica E **6**, 817 (2000)] over the whole temperature regime (from 20 K to 300 K). The value of the fitted spin splitting parameter agrees with many experiments and theoretical calculations. We further show the temperature dependence of the spin relaxation time under various conditions such as electron density, impurity density and well width. We predict a peak solely due to the Coulomb scattering in the spin relaxation time at low temperature (< 50 K) in samples with low electron density (*e.g.*, density less than $1 \times 10^{11} \text{ cm}^{-2}$) but high mobility. This peak disappears in samples with high electron density (*e.g.* $2 \times 10^{11} \text{ cm}^{-2}$) and/or low mobility. The hot-electron spin kinetics at low temperature is also addressed with many features quite different from the high temperature case predicted.

PACS numbers: 72.25.Rb, 72.20.Ht, 71.10.-w, 67.57.Lm

I. INTRODUCTION

Much attention has been devoted to the electron spin dynamics in semiconductors for the past three decades.^{1,2} Especially, recent experiments have shown extremely long spin lifetime (up to hundreds of nanoseconds) in n -type bulk Zinc-blende semiconductors (such as GaAs).^{3,4,5} Moreover, a lot more investigations have been performed on various low dimensional systems,^{6,7,8,9,10,11,12,13,14,15,16,17,18,19,20} and spin lifetime as long as tens of nanoseconds has been reported in (110)-oriented GaAs quantum wells (QWs)^{14,15} at room temperature and in p -type GaAs:Be/ $\text{Al}_x\text{Ga}_{1-x}\text{As}$ double hetero-structures⁷ at low temperature. In these studies, understanding the spin relaxation/dephasing (R/D) mechanism is one of the most important problems as it is the prerequisite for the application of the spintronic devices. It is understood that the D'yakonov-Perel' (DP) mechanism is the leading spin R/D mechanism in n -type Zinc-blende semiconductors.²¹ This mechanism is composed of the contribution from the Dresselhaus term,²² which is due to the lack of inversion symmetry in the Zinc-blende crystal Brillouin zone (sometimes referred to as the bulk inversion asymmetry), and that from the Rashba term,²³ which originates from the asymmetric potential within a QW along the growth direction (sometimes referred to as the structure inversion asymmetry). Both appear as effective magnetic fields. For narrow (001) GaAs QW without the additional large bias voltage, the Dresselhaus term is the leading term.^{24,25}

$$\Omega_x(\mathbf{k}) = \gamma k_x (k_y^2 - \langle k_z^2 \rangle), \quad (1)$$

$$\Omega_y(\mathbf{k}) = \gamma k_y (\langle k_z^2 \rangle - k_x^2), \quad (2)$$

$$\Omega_z(\mathbf{k}) = 0, \quad (3)$$

in which $\langle k_z^2 \rangle$ represents the average of the operator $-(\partial/\partial z)^2$ over the electronic state of the lowest subband. Under the finite square well assumption,

$$\langle k_z^2 \rangle = \frac{4A}{a^2} \left(2\beta + \frac{\xi^2}{\cos^2 \xi} \right), \quad (4)$$

where ξ and β are the lowest energy solutions of the equations

$$\begin{aligned} \beta &= \xi \tan \xi \\ \xi^2 + \beta^2 &= m^* V a^2 / 2\hbar^2, \end{aligned} \quad (5)$$

and $A = \left(\frac{1}{\beta} + \frac{1}{\cos^2 \xi} + \frac{\beta}{\xi^2} \right)^{-1}$ with V , a and m^* denoting the well depth, well width and the effective mass respectively. In the limiting case, $\lim_{V \rightarrow \infty} \langle k_z^2 \rangle = (\pi/a)^2$. γ is the spin splitting parameter.¹ There are a lot of theoretical investigations on the spin R/D due to the DP mechanism lately.^{26,27,28} Most of them are within the framework of single-particle approximation and the Coulomb scattering is thought to be irrelevant in the spin R/D.

Recently Wu *et al.* performed a full microscopic investigation on the spin R/D and showed that the single-particle approach is inadequate in accounting for the spin R/D.^{29,30,31,32,33,34,35,36,37,38,39,40} In this approach, the momentum dependence of the effective magnetic field (the DP term) and the momentum dependence of the spin diffusion rate in the direction of

the spacial gradient³⁴ or even the random spin-orbit interaction⁴¹ serve as inhomogeneous broadening.^{30,31} In the presence of the inhomogeneous broadening, any scattering (even the spin-conserving scattering), including the Coulomb scattering,^{30,35,36,39} can cause irreversible dephasing. Moreover, this approach also includes the counter effect of the scattering to the inhomogeneous broadening, *i.e.*, the suppression of the inhomogeneous broadening by the scattering. Finally, this approach is valid not only near the equilibrium, but also far away from the equilibrium,^{35,36} and is applicable to both the strong ($|\mathbf{\Omega}|\tau_p \ll 1$) and the weak ($|\mathbf{\Omega}|\tau_p \gg 1$) scattering limits,^{39,40} with τ_p representing the momentum relaxation time. In the weak scattering limit, the counter effect of the scattering is less important and adding additional scattering (including the Coulomb scattering) causes stronger spin R/D. Whereas in the strong scattering limit, adding additional scattering always increases the spin R/D time. The feature is more complicated when $|\mathbf{\Omega}|\tau_p \sim 1$.³⁹ In above studies,^{29,30,31,32,33,34,35,36,37,38,39,40} we have been focusing on the high temperature regime ($T \geq 120$ K) where the electron-acoustic (AC) phonon scattering, which is more complicated in numerical calculation than the electron-longitudinal optical (LO) phonon scattering, is negligible. In this paper, we extend the scope of our approach to study the spin kinetics at low temperature regime by including the electron-AC phonon scattering. Moreover, we compare the spin relaxation time (SRT) obtained from our theory with the experimental data over a wide temperature regime and show the excellent agreement of our theory with the experiment. We further show that the Coulomb scattering is important to the spin R/D not only at high temperatures,^{35,36,39} but also at low temperatures. The electron density, impurity density, well width, temperature and electric field dependences of the SRT are studied in detail.

This paper is organized as follows: In Sec. II we set up the model and give the kinetic spin Bloch equations. In Sec. III we compare our results with the experimental data. Then, we investigate the temperature dependence of the spin relaxation under different conditions such as electron densities, impurity densities and well widths in Sec. IV. The effect of Coulomb scattering is also addressed. The hot-electron effect in spin relaxation is investigated in Sec. V. We summarize in Sec. VI.

II. KINETIC SPIN BLOCH EQUATIONS

We start our investigation from an n -type GaAs (001) QW with the growth direction along the z -axis. A moderate magnetic field B is applied along the x -axis (in the Voigt configuration). The kinetic spin Bloch equations can be constructed by using the nonequilibrium Green function method.⁴²

$$\dot{\rho}_{\mathbf{k},\sigma\sigma'} - e\mathbf{E} \cdot \nabla_{\mathbf{k}} \rho_{\mathbf{k},\sigma\sigma'} = \dot{\rho}_{\mathbf{k},\sigma\sigma'}|_{coh} + \dot{\rho}_{\mathbf{k},\sigma\sigma'}|_{scatt}, \quad (6)$$

with $\rho_{\mathbf{k},\sigma\sigma'}$ representing the single particle matrix elements. The diagonal and off-diagonal elements give the electron distribution functions $f_{\mathbf{k}\sigma}$ and the spin coherence $\rho_{\mathbf{k},\sigma-\sigma}$. The second term in Eq. (6) describes the energy input from the external electric field \mathbf{E} . The coherent terms $\dot{\rho}_{\mathbf{k},\sigma\sigma'}|_{coh}$ describe the precession of the electron spin due to the applied magnetic field B and the effective magnetic field $\mathbf{\Omega}(\mathbf{k})$ [Eqs. (1-3)] as well as the effective magnetic field from the Hartree-Fock Coulomb interaction.³⁵ $\dot{\rho}_{\mathbf{k},\sigma\sigma'}|_{scatt}$ in Eq. (6) denote the electron-LO-phonon, the electron-AC-phonon, the electron-nonmagnetic impurity and the electron-electron Coulomb scattering. Their expressions are given in detail in Ref. 36, except the additional matrix elements of the electron-AC-phonon scattering. For the electron-AC-phonon scattering due to the deformation potential, the matrix elements are given by $g_{\mathbf{Q},def}^2 = \frac{\hbar^2 \Xi^2 Q}{2d v_{st}} |I(iq_z)|^2$,⁴³ and for the scattering due to the piezoelectric coupling, the matrix elements read $g_{\mathbf{Q},pl}^2 = \frac{32\pi^2 \hbar^2 e_{14}^2}{\kappa_0^2} \frac{(3q_x q_y q_z)^2}{d v_{st} Q^7} |I(iq_z)|^2$ for the longitudinal phonon and $g_{\mathbf{Q},pt}^2 = \frac{32\pi^2 \hbar^2 e_{14}^2}{\kappa_0^2} \frac{1}{d v_{st} Q^5} (q_x^2 q_y^2 + q_y^2 q_z^2 + q_z^2 q_x^2 - \frac{(3q_x q_y q_z)^2}{Q^2}) |I(iq_z)|^2$ for the transverse phonon.⁴⁴ Here $\mathbf{Q} \equiv (\mathbf{q}, q_z)$; $Q = \sqrt{q_x^2 + q_y^2 + q_z^2}$; $\Xi = 8.5$ eV is the deformation potential; $d = 5.31$ g/cm³ is the mass density of the crystal; $v_{st} = 5.29 \times 10^3$ m/s ($v_{st} = 2.48 \times 10^3$ m/s) is the velocity of the longitudinal (transverse) sound wave; $\kappa_0 = 12.9$ denotes the static dielectric constant; and $e_{14} = 1.41 \times 10^9$ V/m represents the piezoelectric constant.⁴⁵ The AC phonon spectra $\omega_{\mathbf{Q}\lambda}$ are given by $\omega_{\mathbf{Q}l} = v_{st} Q$ for the longitudinal mode and $\omega_{\mathbf{Q}t} = v_{st} Q$ for the transverse mode. The form factor is

$$|I(iq_z)|^2 = A^2 \left\{ \frac{4\beta \cos y - y \sin y}{4\beta^2 + y^2} + \frac{1}{\cos^2 \xi} \times \left[\frac{\sin y}{y} + \frac{\sin(y + 2\xi)}{2y + 4\xi} + \frac{\sin(y - 2\xi)}{2y - 4\xi} \right] \right\}^2 \quad (7)$$

with $y = q_z a/2$. The numerical schemes of the electron-electron Coulomb, the electron-impurity as well as the electron-LO phonon scattering have been given in detail in Ref. 36, whereas the numerical scheme for the electron-AC-phonon scattering is presented in Appendix A. The electron-interface-phonon scattering is negligible due to the thick GaAlAs barrier. In addition, as we are going to explore the spin R/D over a wide range of electron densities, in the present paper we use the screening under the random phase approximation⁴⁶ rather than the one in the limiting (degenerate or nondegenerate) cases for the screened Coulomb potential.⁴⁷

$$\bar{v}_q = \frac{\sum_{q_z} v_Q |I(iq_z)|^2}{1 - \sum_{q_z} v_Q |I(iq_z)|^2 P^{(1)}(\mathbf{q})}, \quad (8)$$

where $v_Q = 4\pi e^2 / Q^2$ is the bare Coulomb potential and

$$P^{(1)}(\mathbf{q}) = \sum_{\mathbf{k},\sigma} \frac{f_{\mathbf{k}+\mathbf{q}\sigma} - f_{\mathbf{k}\sigma}}{\epsilon_{\mathbf{k}+\mathbf{q}} - \epsilon_{\mathbf{k}}}. \quad (9)$$

In this way, we also take into account the hot-electron effect on the screening.

By numerically solving the kinetic spin Bloch equations with all these scattering explicitly included, one is able to obtain the spin dephasing and relaxation times from the temporal evolutions of the spin coherence $\rho_{\mathbf{k},\sigma-\sigma}$ and the electron distribution functions $f_{\mathbf{k},\sigma}$. The irreversible spin dephasing time can be obtained by the slope of the envelope of the incoherently summed spin coherence²⁹ $\rho = \sum_{\mathbf{k}} |\rho_{\mathbf{k},\uparrow\downarrow}(t)|$, and the SRT can be defined by the slope of the envelope of the difference between n_{\uparrow} and n_{\downarrow} , with $n_{\sigma} = \sum_{\mathbf{k}} f_{\mathbf{k},\sigma}$.

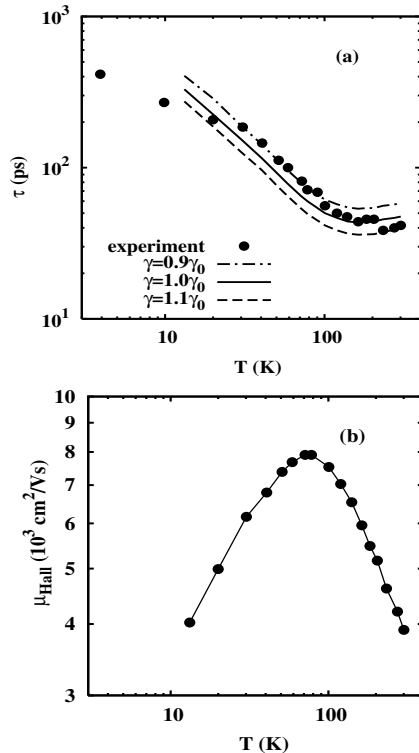


FIG. 1: (a) SRT τ vs. temperature T for GaAs QW with $a = 7.5$ nm and electron density $n = 4 \times 10^{10} \text{ cm}^{-2}$ at three different spin-splitting parameters. Dots: experiment data; Dot-dashed curve: $\gamma = 0.9\gamma_0$; Solid curve: $\gamma = \gamma_0$; Dashed curve: $\gamma = 1.1\gamma_0$. (b) Hall mobility μ_{Hall} vs. temperature T (Ref. 12).

III. COMPARISON WITH EXPERIMENT

First, we compare the SRT obtained from our microscopic approach with the experimental data by Ohno *et al.* in 60 periods of GaAs QWs separated by 10 – 12 nm thick $\text{Al}_{0.4}\text{Ga}_{0.6}\text{As}$ barriers. The well width of each QW $a = 7.5$ nm and the electron density $n = 4 \times 10^{10} \text{ cm}^{-2}$.¹² The well depth of the GaAs well confined by $\text{Al}_x\text{Ga}_{1-x}\text{As}$ is roughly estimated to be 65 % of $1.087x + 0.438x^2$ eV, for $x = 0.4$ and is therefore $V_0 = 328$ meV.⁴⁸ Differently from our previous fit³⁵ with the experiment data at high

temperatures by Malinowski *et al.*¹³ where we had two fitting parameters, *i.e.*, the spin splitting parameter γ and the impurity density n_i due to the absence of mobility data, here we have only one fitting parameter γ and the temperature sweeps from the very low temperature to the room temperature. The corresponding Hall mobilities μ_{Hall} in the experiment¹² can be found in Ref. 27, also plotted in Fig. 1(b). From the Hall mobility, one can deduce the impurity density by calculating the transport mobilities⁴⁹ $\mu_{tr} = \mu_{\text{Hall}}/r_{\text{Hall}}$ with $r_{\text{Hall}} = 1$ for the electron-AC phonon scattering due to the deformation potential; $r_{\text{Hall}} = 7/5$ for the electron-AC phonon scattering due to the piezoelectric coupling and the electron-LO phonon scattering; and $r_{\text{Hall}} = 1$ for the electron-ionized impurity scattering.⁵⁰

The only fitting parameter γ is around

$$\gamma = (4/3)(m^*/m_{cv})(1/\sqrt{2m^*E_g})(\eta/\sqrt{1-\eta/3}), \quad (10)$$

in which $\eta = \Delta/(E_g + \Delta)$; E_g denotes the band gap; Δ represents the spin-orbit splitting of the valence band; m^* stands for the electron mass in GaAs; and m_{cv} is a constant close in magnitude to the free electron mass m_0 .⁵¹ For GaAs when $m_{cv} = m_0$, $\gamma = \gamma_0 = 11.4 \text{ eV}\cdot\text{\AA}^3$. The initial spin polarization P is assumed to be 2.5 % for weak polarization throughout the paper. In Fig. 1(a), the SRTs τ obtained from our approach are plotted against the temperature with all the scattering included. B and E are taken to be zero, as in the experiment.¹² $\gamma = 0.9, 1.0$ and $1.1\gamma_0$ correspond to $m_{cv} = 1.1, 1.0$ and $0.91m_0$ with m_{cv} being the only not-fully-determined parameter in Eq. (10). One finds *good* agreement between our theory and the experiment data almost over the *whole* temperature regime. When T is below 13 K, there is no theoretical data due to the lack of experimental data for the Hall mobility. Kainz *et al.* also fitted the same experiment data by using the single-particle theory without the Coulomb scattering.²⁷ They used a fourteen-band model to calculate the spin-orbit coupling. Unlike our theory, their results can only give the boundary values of the SRT in several cases rather than the exact data.²⁷ This is because they did not take the full microscopic calculation, and the single-particle theory is inadequate in accounting for the spin R/D.

The best-fitted value of the spin-orbit coupling parameter, *i.e.*, $\gamma_0 = 11.4 \text{ eV}\cdot\text{\AA}^3$, is close to the value calculated by Kainz *et al.* ($\sim 16.5 \text{ eV}\cdot\text{\AA}^3$) using the multiband envelope-function approximation.²⁷ It is noted that the value for γ in GaAs is still in debate. Usually reported experimental values for γ (25 – 30 $\text{eV}\cdot\text{\AA}^3$) in bulk material are deduced from the DP spin relaxation mechanism within the framework of the single-particle approximation, where the Coulomb scattering is not included.⁵² Furthermore, the Raman scattering experiment showed that $\gamma = 16.5 \pm 3 \text{ eV}\cdot\text{\AA}^3$ in asymmetric QW;⁵³ and the Hanle effect experiment showed that $\gamma = 12.6 \text{ eV}\cdot\text{\AA}^3$.⁵⁴ Theoretically, semi-empirical parameterized 16×16 $\mathbf{k}\cdot\mathbf{p}$ calculations show that $\gamma = 14.9$

$\text{eV}\cdot\text{\AA}^3$;⁵⁵ and the self-consistent *ab initio* calculations predict 6.4 and 8.5 $\text{eV}\cdot\text{\AA}^3$.⁵⁶ Our fitting result supports the last four experimental and theoretical results. It is also noted that our result further confirms the analytical result Eq. (10) obtained from the perturbation,⁵¹ with $m_{cv} = m_0$.

IV. TEMPERATURE DEPENDENCE OF SRT

We now study the temperature dependence of the spin relaxation in detail. In the calculation, the electric field $E = 0$, the magnetic field $B = 0$ T and the spin splitting parameter $\gamma = \gamma_0$.

We plot in Fig. 2 the temperature dependence of the SRT of GaAs/Al_{0.4}Ga_{0.6}As QWs with $a = 7.5$ nm at different impurity densities when the electron densities are low ($n = 4 \times 10^{10} \text{ cm}^{-2}$) [Fig. 2(a)], medium ($n = 1 \times 10^{11} \text{ cm}^{-2}$) [Fig. 2(b)] and high ($n = 2 \times 10^{11} \text{ cm}^{-2}$) [Fig. 2(c)] respectively as solid curves. For the well width and the electron densities here, the linear terms in the DP terms [Eqs. (1-3)] are dominant, and only the lowest subband is relevant when $T \leq 300$ K. It is seen from the figure that adding impurities always increases the SRT. This is understood that the criterion of strong scattering $|\Omega|\tau_p \ll 1$ is satisfied here at all temperatures, and therefore adding additional scattering always increases the SRT.³⁹ It is noted that τ_p here has been extended to include τ_p^{ee} , *i.e.*, the contribution from the Coulomb scattering.⁵⁷ It is interesting to note that unlike our previous works focusing on high temperatures ($T \geq 120$ K),^{32,33,34,35,36,37,38,39,40} the situation is more complicated at low temperatures. At low/medium electron densities [Fig. 2(a)/(b)], the SRT presents a peak at very low temperature (near 20~30 K)/low temperature (around 41 K) and a valley around 120 K; whereas at high electron density [Fig. 2(c)], the SRT increases monotonically with T .

It is noted that at very low temperature (around 20 K) the electron-AC phonon scattering is negligible.⁵⁸ τ_p^{AC} from the electron-AC phonon scattering is around 25 ps, two orders of magnitude larger than τ_p^{ee} from the electron-electron Coulomb scattering. In addition, τ_p^i from the impurity scattering is around 2 ps, one order of magnitude larger than τ_p^{ee} , and has a very weak temperature dependence. Therefore, the appearance of the peaks in Fig. 2(a) originates from the electron-electron Coulomb scattering which dominates the scattering process. Moreover, τ_p^{ee} is a nonmonotonic function of temperature: $\tau_p^{ee} \propto T^{-2}$ at low temperature (degenerate limit) and $\tau_p^{ee} \propto T$ at high temperature (nondegenerate limit).⁵⁹ The minimum of τ_p^{ee} corresponds to the crossover from the degenerate limit to the nondegenerate one at $T_c \sim E_F/k_B$. $T_c \sim 17$ K when $n = 4 \times 10^{10} \text{ cm}^{-2}$, in good agreement with the peaks obtained from our calculation with the exact Coulomb scattering. Therefore the SRT increases/decreases with

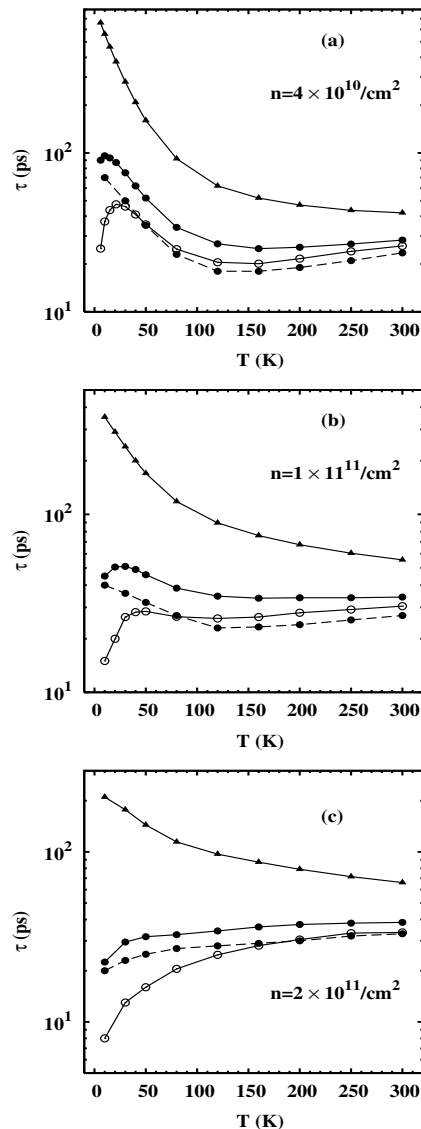


FIG. 2: SRT τ vs the temperature T with well width $a = 7.5$ nm and electron density n being (a) $4 \times 10^{10} \text{ cm}^{-2}$, (b) $1 \times 10^{11} \text{ cm}^{-2}$ and (c) $2 \times 10^{11} \text{ cm}^{-2}$ respectively. Solid curve with triangles: $n_i = n$; Solid curve with dots: $n_i = 0.1n$; Solid curve with circles: $n_i = 0$; Dashed curve with dots: $n_i = 0.1n$ and no Coulomb scattering.

the temperature (and the Coulomb scattering) in the degenerate/nondegenerate regime. Once $T \geq 120$ K, the electron-LO phonon scattering becomes comparable with the Coulomb scattering and strengthens so rapidly with temperature that it completely surpasses the weak temperature dependence of the Coulomb scattering: τ_p^{LO} from the electron-LO phonon scattering varies from several picoseconds at 120 K to several tenths of picosecond at 300 K, and τ_p^{ee} varies from 1 ps to several picoseconds. Therefore the SRT increases with T . When the electron density is $1 \times 10^{11} \text{ cm}^{-2}$, T_c is nearly 41 K. Around this temperature, the electron-AC phonon scattering cannot

be overlooked although τ_p^{AC} is still roughly one order of magnitude larger than τ_p^{ee} . Therefore, the reduction of the Coulomb scattering after T_c can be partly compensated by the increase of the electron-phonon scattering. As a result, one can see that the decrease of the SRT after T_c in Fig. 2(b) is much slower than that in Fig. 2(a). However, when the electron density is high enough, say $2 \times 10^{11} \text{ cm}^{-2}$ in Fig. 2(c), T_c is nearly 83 K, much larger than the case of low electron density. At this temperature, the electron-phonon scattering becomes comparable to the Coulomb scattering and the strengthening rate of phonon scattering around this temperature is large enough to completely compensate, and even surpass, the weakening rate of the Coulomb scattering. Consequently the total scattering increases monotonously with T . Therefore the SRT increases monotonically with T .

We further show the effect of the Coulomb scattering on the spin relaxation. This was first proposed by Wu and Ning based on the inhomogeneous broadening induced by the energy dependence of the g -factor.³⁰ Then, we used our full microscopic approach and showed that the Coulomb scattering makes marked contribution to the spin R/D when $T \geq 120$ K when the inhomogeneous broadening is induced by the DP term.^{35,36,39} At low temperature ($T < 120$ K), Glazov and Ivchenko used perturbation method to show that the second-order Coulomb scattering causes the SRT.⁶⁰ In the perturbation approach, the Coulomb scattering contributes marginally to the spin R/D at high temperature. In our calculation, we include the Coulomb scattering to all orders of the bubble diagrams as well as the counter effect of the Coulomb scattering to the inhomogeneous broadening. In Fig. 2 by plotting the SRT for the case of $n_i = 0.1n$, but without the Coulomb scattering, as dashed curves, we show that the Coulomb scattering makes marked contribution to the spin R/D over the whole temperature regime by increasing the spin R/D time.⁶¹ It is further seen from Figs. 2(a) and (b) that the peak disappears without the Coulomb scattering. This is consistent with the previous discussion.

It is interesting to see that in the absence of the Coulomb scattering, the criterion for strong scattering regime $|\Omega|\tau_p \ll 1$ is satisfied only when $T > 120$ K. Therefore the SRT increases with T when $T \geq 120$ K. When $T < 120$ K, $|\Omega|\tau_p$ is slightly smaller than 1, which is the intermediate scattering regime. The variation of the SRT depends on the competition between the increase of the inhomogeneous broadening and the increase of the scattering with the temperature.³⁹ For low/high electron density case, the temperature dependence of the electron-AC phonon scattering is less/more effective and the SRT decreases/increases with T .

It is noted that in order to see the peaks at low electron density, it is important to have a high mobility sample (low impurity density). This is because the ascendancy of the Coulomb scattering can be impaired when the impurity scattering gets large enough and the total scattering is mainly determined by the impurity scattering. As the

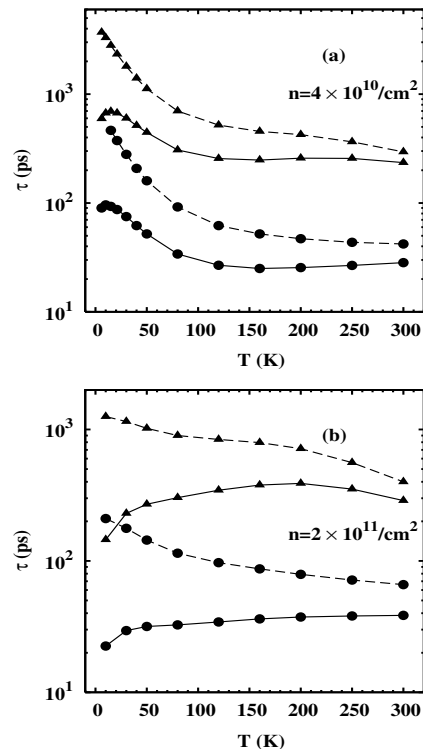


FIG. 3: SRT τ vs. temperature T at $a = 7.5$ nm (curves with dots) and 15 nm (curves with triangles). Solid curves: $n_i = 0.1n$; Dashed curves: $n_i = n$. (a) $n = 4 \times 10^{10} \text{ cm}^{-2}$ and (b) $n = 2 \times 10^{11} \text{ cm}^{-2}$.

electron-impurity scattering depends weakly on the temperature, the temperature dependence of the inhomogeneous broadening from the DP term becomes the only variable element. Therefore the SRT decreases monotonically with T as the solid curves with triangles in Fig. 2 for the case of $n_i = n$. This condition is not satisfied in the experiment by Ohno *et al.*,¹² and this is the reason why there is no peak in Fig. 1. However, apart from the peaks which are not observed yet, both the experiment and calculation show that the SRT decreases with temperature at low electron densities when $T < 120$ K. The SRT at high electron density increases monotonically with temperature when the impurity density is low, which is also in agreement with the latest experiment by Harley *et al.*⁶²

Finally we investigate the well width dependence of the SRT. In Fig. 3 we plot the SRT versus temperature at well widths $a = 7.5$ nm (solid curves) and 15 nm (dashed curves) respectively. We choose low and high impurity densities $n_i = 0.1n$ (curves with dots) and $n_i = n$ (curves with triangles) as well as low and high electron densities $n = 4 \times 10^{10} \text{ cm}^{-2}$ (a) and $n = 2 \times 10^{11} \text{ cm}^{-2}$ (b). It is noted that the SRT is enhanced by increasing the well width as $\langle k_z^2 \rangle$ in the DP term decreases with the increase of a . Moreover, as impurities further enhance the SRT, it reaches to several nanoseconds at very low temperatures at high impurity density.

V. ELECTRIC FIELD DEPENDENCE OF SRT

We now turn to investigating the hot-electron effect on spin relaxation at low temperature. An electric field is applied parallel to the QW. Similar to our previous investigation,³⁶ electrons obtain a center-of-mass drift velocity (and consequently an effective magnetic field proportional to the electric field) and are heated to a temperature T_e higher than T . The numerical schemes of solving the hot electron problem has been laid out in detail in Ref. 36.⁶³ We plot the electric field dependence of the SRT with $a = 7.5$ nm and $T = 50$ K for different impurity densities at low/high electron density ($n = 4 \times 10^{10}$ cm⁻²/ $n = 2 \times 10^{11}$ cm⁻²) in Fig. 4(a)/(b). In the calculation, the magnetic field $B = 4$ T and the spin splitting parameter $\gamma = \gamma_0$ as in the previous section. It is seen from the figure that unlike the high temperature case investigated before³⁶ (and also see Fig. 4(c) for $T = 120$ K) where the electric field can be applied easily to around 1 kV/cm, at low temperatures it can be applied only to a very small value due to the “runaway” effect.⁶⁴ This is because at low temperature, the efficient electron-LO phonon scattering is missing and electrons are therefore very easily driven to very high momentum states by a very small electric field.

It is interesting to see from the figure that differing from the high temperature case where the SRT *increases* with the electric field (see Fig. 4 (c) and also Ref. 36), here, for the case of low electron densities, the SRT *decreases* with the field and for the case of high electron densities, the SRT decreases/increases with the field at high/low impurity densities.

These features at low temperature T can be understood from the joint effects of the electric field E to the scattering strength and the inhomogeneous broadening due to the DP term. On one hand, when the electric field is small, the ionized-impurity scattering, whose strength decreases slightly with the electron temperature T_e , is dominant. When the electric field is further increased, T_e and therefore the electron-AC phonon scattering is raised. If the impurity scattering is not too high, the electron-AC phonon scattering can then be dominant as discussed decades ago in Ref. 65. These can be seen from the mobilities $\mu = \sum_{\mathbf{k}\sigma} \hbar \mathbf{k} f_{\mathbf{k}\sigma} / (m^* n E)$ obtained from our calculation, which are plotted in the same figure for all the corresponding cases. One can see that μ increases slightly and monotonically with E for the impurity-scattering-dominant case such as $n_i = n$; It decreases monotonically with E for the case of very low/no impurity scattering such as $n_i = 0$, as the electron-AC phonon scattering always increases with the electron temperature T_e ; for the case of low impurity scattering such as $n_i = 0.1n$, μ first increases slightly then decreases with E which shows the transition from the impurity-scattering-dominant regime to the electron-AC-phonon-scattering-dominant regime⁶⁵ (unless the runaway effect blocks the system to the later regime as shown in Fig. 4(a) for the case of low electron densities). On the other

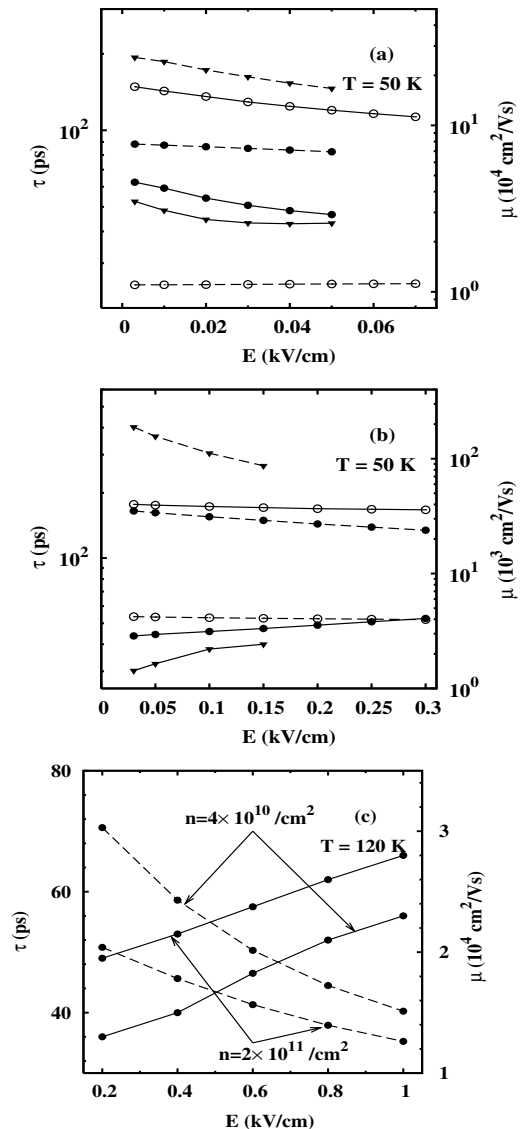


FIG. 4: SRT τ (solid curves) and mobility μ (dashed curves) vs. electric field E . (a) $T = 50$ K and $n = 4 \times 10^{10}$ cm⁻²; (b) $T = 50$ K and $n = 2 \times 10^{11}$ cm⁻²; (c) $T = 120$ K, $n = 4 \times 10^{10}$ cm⁻² and 2×10^{11} cm⁻² respectively. Curves with open circles: $n_i = n$; with dots: $n_i = 0.1n$; with triangles: $n_i = 0$. Note the scales of the mobility μ are on the right side of the figures.

hand, electrons are driven to the higher momentum states by the electric field and experience a larger effective magnetic field [Eqs. (1-3)]. Therefore the inhomogeneous broadening is increased. This tends to decrease the SRT. In order to show the electric field dependence of the inhomogeneous broadening, we plot in Fig. 5 the electron temperature T_e as a function of electric field E for all the corresponding cases in Figs. 4(a) and (b). It is obvious from Fig. 5 that the increase of T_e for the low electron density case is much faster than that for the high one. Therefore, the increase of the inhomogeneous broadening

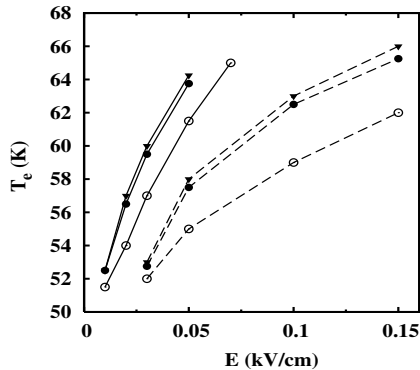


FIG. 5: Hot electron temperature T_e vs. electric field E when $T = 50$ K. solid curves: $n = 4 \times 10^{10} \text{ cm}^{-2}$; dashed curves: $n = 2 \times 10^{11} \text{ cm}^{-2}$. Curves with open circles: $n_i = n$; with dots: $n_i = 0.1n$; with triangle: $n_i = 0$.

is the leading contribution in comparison with the electric field effect on the scattering. Consequently, the SRT decreases with E for the case of low electron densities as shown in Fig. 4(a). For the case of high electron densities, when the impurity density is high such as $n_i = n$ in Fig. 4(b), both the slight decrease of the scattering and the increase of the inhomogeneous broadening tend to suppress the SRT. When the impurity density is low/zero, the strengthening of the scattering is dominant (as shown in Fig. 4(b) the decrease of mobility with E) in comparison with the increase of the inhomogeneous broadening. This makes the SRT decrease with E . Finally we point out that the Coulomb scattering plays an essential role in the spin R/D in the presence of the electric field. It determines the hot-electron temperature T_e which controls the inhomogeneous broadening and the scattering strengths. Moreover, the Coulomb scattering itself also contributes to the spin R/D.

For comparison, we also plot the SRT versus electric field at high temperature $T = 120$ K for both low and high electron densities with $n_i = 0.1n$ in Fig. 4(c). At this temperature, the electron-LO phonon scattering is dominant. Therefore μ always decrease with E . For the well width and electron density we study, the linear DP term is dominant and the increase of the scattering is more important. Therefore the SRT increases with E . For QWs with larger well width so that the cubic term is dominant, the SRT can decrease with E as reported in our previous work at high temperatures.³⁷

VI. SUMMARY

In summary, we have investigated the temperature dependence of the SRT for n -type GaAs (001) QWs with small well widths from a full microscopic approach by constructing and numerically solving the kinetic spin Bloch equations with all the relevant scattering explicitly included. In contrast to our previous studies at high

temperatures ($T \geq 120$ K), we include the electron-AC phonon scattering which is absent in our previous studies so that we may extend the scope of our approach to the low temperature regime ($T < 120$ K). Good agreement with experiment data¹² is obtained from our theory over almost the *whole* temperature regime by using only one fitting parameter γ whose value agrees with many experimental and theoretical results. We show that the Coulomb scattering plays an essential role in spin R/D over all the temperature regime.

For QWs with low electron densities but high mobility (*i.e.*, low impurity density), the spin R/D is mainly controlled by the electron-electron Coulomb scattering when $T < 70$ K. We predict a peak in the τ - T curve. The closer the peak approaches the high temperature limit, the smoother the peak appears. After the peak, the SRT increases with temperature. Finally, such a peak disappears at sufficient high electron density where the SRT increases monotonically with temperature. We point out that the peak origins from the Coulomb scattering. Specifically, it origins from the different temperature dependences of the Coulomb scattering at the degenerate and the nondegenerate limits with the transition temperature $T_c \sim E_F/k_B$. For low electron densities, $T_c \leq 30$ K where the electron-phonon scattering is negligible. Then one may observe an abrupt peak around T_c . For medium electron densities, $30 \text{ K} < T_c < 70$ K where the increase of the electron-AC phonon scattering partially compensates the decrease of the Coulomb scattering when T increases, one may observe a smooth peak around T_c . Nevertheless, for high electron densities, $T_c > 70$ K, the increase of the electron-phonon scattering completely compensates the decrease of the Coulomb scattering when T rises. Consequently the peak disappears.

At high temperature ($T \geq 120$ K) and low impurity density, when the well width is small so that the cubic terms in the DP terms are unimportant, the increase of electron-LO phonon scattering surpasses the increase of inhomogeneous broadening with temperature, so that the SRT increases with temperature. However, when the impurity density is so high that electron-impurity scattering is the dominant scattering mechanism, the SRT decreases monotonically with temperature for any electron density. This is because the temperature dependence of the electron-impurity scattering is very weak and the increase of the inhomogeneous broadening with temperature dominates the temperature dependence of the SRT. We also show that larger well width leads to a slower spin relaxation. Moreover, in the strong scattering limit, higher impurity density also leads to a slower spin relaxation. Both effects can make the SRT as long as nanoseconds at very low temperatures.

The effect of electric field (*i.e.*, the hot electron effect) on the spin relaxation is also investigated. We show that the electric field dependence of the SRT at low temperature appears again quite differently from that at high temperature due to the absence of electron-LO phonon scattering. Moreover, we further show different electric

field dependences of the SRT at low and high electron densities. At low electron densities, the SRT *decreases* with the electric field. When the electron density is high, it *decreases/increases* with the electric field for the case of high/low impurity densities. These features are in giant difference from the high temperature case where the SRT *increases* monotonically with electric field for the same QWs. More experiments are needed to explore the predictions presented in this manuscript.

Acknowledgments

This work was supported by the Natural Science Foundation of China under Grant Nos. 90303012 and

10574120, the Natural Science Foundation of Anhui Province under Grant No. 050460203, the Knowledge Innovation Project of Chinese Academy of Sciences and SRFDP. The authors would like to thank I. C. da Cunha Lima for his critical reading of this manuscript to improve the English.

APPENDIX A: NUMERICAL SCHEME FOR ELECTRON-AC PHONON SCATTERING

The electron-AC phonon scattering terms can be rewritten as

$$\left. \frac{\partial f_{\mathbf{k},\sigma}}{\partial t} \right|_{\text{AC}} = \left\{ -2\pi \sum_{\mathbf{q}q_z,\lambda} g_{\mathbf{q}q_z,\lambda}^2 \delta(\epsilon_{\mathbf{k}} - \epsilon_{\mathbf{k}-\mathbf{q}} - \Omega_{\mathbf{q}q_z,\lambda}) [N(\epsilon_{\mathbf{k}} - \epsilon_{\mathbf{k}-\mathbf{q}})(f_{\mathbf{k},\sigma} - f_{\mathbf{k}-\mathbf{q},\sigma}) + f_{\mathbf{k},\sigma}(1 - f_{\mathbf{k}-\mathbf{q},\sigma}) - \text{Re}(\rho_{\mathbf{k}}\rho_{\mathbf{k}-\mathbf{q}}^*)] \right\} - \left\{ \mathbf{k} \leftrightarrow \mathbf{k} - \mathbf{q} \right\}, \quad (\text{A1})$$

$$\left. \frac{\partial \rho_{\mathbf{k}}}{\partial t} \right|_{\text{AC}} = \left\{ \pi \sum_{\mathbf{q}q_z,\lambda} g_{\mathbf{q}q_z,\lambda}^2 \delta(\epsilon_{\mathbf{k}} - \epsilon_{\mathbf{k}-\mathbf{q}} - \Omega_{\mathbf{q}q_z,\lambda}) [\rho_{\mathbf{k}-\mathbf{q}}(f_{\mathbf{k},\uparrow} + f_{\mathbf{k},\downarrow}) + (f_{\mathbf{k}-\mathbf{q},\uparrow} + f_{\mathbf{k}-\mathbf{q},\downarrow} - 2)\rho_{\mathbf{k}} - 2N(\epsilon_{\mathbf{k}} - \epsilon_{\mathbf{k}-\mathbf{q}})(\rho_{\mathbf{k}} - \rho_{\mathbf{k}-\mathbf{q}})] \right\} - \left\{ \mathbf{k} \leftrightarrow \mathbf{k} - \mathbf{q} \right\}, \quad (\text{A2})$$

with $\rho_{\mathbf{k}} \equiv \rho_{\mathbf{k},\uparrow\downarrow}$ and $\{\mathbf{k} \leftrightarrow \mathbf{k} - \mathbf{q}\}$ standing for the same terms as the previous $\{\}$ but with the interchange $\mathbf{k} \leftrightarrow \mathbf{k} - \mathbf{q}$. $N(\epsilon_{\mathbf{k}} - \epsilon_{\mathbf{k}-\mathbf{q}}) = [\exp\{\beta(\epsilon_{\mathbf{k}} - \epsilon_{\mathbf{k}-\mathbf{q}})\} - 1]^{-1}$ represents the Bose distribution. The division of the truncated two-dimensional momentum space is all the same as our previous work (see Fig. 8 in Ref. 36). The two dimensional momentum space is thus divided into $N \times M$ control regions, each with the same energy and angle intervals. The \mathbf{k} -grid point of each control region is chosen to be the center of the region:

$$\mathbf{k}_{n,m} = \sqrt{2m^*E_n}(\cos\theta_m, \sin\theta_m), \quad (\text{A3})$$

with $E_n = (n + 1/2)\Delta_E$ and $\theta_m = m\Delta\theta$. $n = 0, 1, \dots, N - 1$ and $m = 0, 1, \dots, M - 1$. with the truncation energy $E_{cut} = E_N$ and $\theta_M = (M - 1)2\pi/M$.

Unlike the electron-LO phonon scattering where the δ -function in the scattering is used to carry out the integral of \mathbf{k}' , more specifically $\theta_{\mathbf{k}'}$, with $\mathbf{k}' \equiv \mathbf{k} - \mathbf{q}$, here the δ -function is used to perform the integral of q_z with

$$q_z = \sqrt{\left(\frac{\epsilon_{\mathbf{k}} - \epsilon_{\mathbf{k}'}}{v_\lambda}\right)^2 - \mathbf{q}^2}. \quad (\text{A4})$$

* Author to whom all correspondence should be addressed; Electronic address: mwwu@ustc.edu.cn.

† Mailing Address.

¹ *Optical Orientation*, edited by F. Meier and B. P. Zakharchenya, (North-Holland, Amsterdam, 1984).

² *Semiconductor Spintronics and Quantum Computation*, eds. D. D. Awschalom, D. Loss, and N. Samarth (Springer, Berlin, 2002); I. Žutić, J. Fabian, and S. Das Sarma, *Rev. Mod. Phys.* **76**, 323 (2004).

³ J. M. Kikkawa and D. D. Awschalom, *Phys. Rev. Lett.* **80**, 4313 (1998).

⁴ R. I. Dzhioev, B. P. Zakharchenya, V. L. Korenev, D. Gammon, and D. S. Katzer, *Pis'ma Zh. Éksp. Teor. Fiz.* **74**, 200

(2001) [*JETP Lett.* **74**, 182 (2001)]; R. I. Dzhioev, K. V. Kavokin, M. V. Lazarev, B. Ya. Meltser, M. N. Stepanova, B. P. Zakharchenya, D. Gammon, and D. S. Katzer, *Phys. Rev. B* **66**, 245204 (2002).

⁵ B. N. Murdin, K. Litvinenko, J. Allam, C. R. Pidgeon, M. Bird, K. Morrison, T. Zhang, S. K. Clowes, W. R. Branford, J. Harries, and L. F. Cohen, *Phys. Rev. B* **72**, 085346 (2005).

⁶ T. C. Damen, L. Viña, J. E. Cunningham, J. Shah, and L. J. Sham, *Phys. Rev. Lett.* **67**, 3432 (1991).

⁷ J. Wagner, H. Schneider, D. Richards, A. Fischer, and K. Ploog, *Phys. Rev. B* **47**, 4786 (1993).

⁸ A. P. Heberle, W. W. Rühle, and K. Ploog, *Phys. Rev.*

- Lett. **72**, 3887 (1994).
- ⁹ S. A. Crooker, J. J. Baumberg, F. Flack, N. Samarth, and D. D. Awschalom, Phys. Rev. Lett. **77**, 2814 (1996); S. A. Crooker, D. D. Awschalom, J. J. Baumberg, F. Flack, and N. Samarth, Phys. Rev. B **56**, 7574 (1997).
 - ¹⁰ J. M. Kikkawa, I. P. Smorchkova, N. Samarth, and D. D. Awschalom, Science **277**, 1284 (1997).
 - ¹¹ Y. Ohno, R. Terauchi, T. Adachi, F. Matsukura, and H. Ohno, Phys. Rev. Lett. **83**, 4196 (1999).
 - ¹² Y. Ohno, R. Terauchi, T. Adachi, F. Matsukura, and H. Ohno, Physica E (Amsterdam) **6**, 817 (2000).
 - ¹³ A. Malinowski, R. S. Britton, T. Grevatt, R. T. Harley, D. A. Ritchie, and M. Y. Simmons, Phys. Rev. B **62**, 13034 (2000); M. A. Brand, A. Malinowski, O. Z. Karimov, P. A. Marsden, R. T. Harley, A. J. Shields, D. Sanvitto, D. A. Ritchie, and M. Y. Simmons, Phys. Rev. Lett. **89**, 236601 (2002).
 - ¹⁴ T. Adachi, Y. Ohno, F. Matsukura, and H. Ohno, Physica E (Amsterdam) **10**, 36 (2001).
 - ¹⁵ O. Z. Karimov, G. H. John, R. T. Harley, W. H. Lau, M. E. Flatté, M. Henini, and R. Airey, Phys. Rev. Lett. **91**, 246601 (2003).
 - ¹⁶ S. Döhrmann, D. Hägele, J. Rudolph, M. Bichler, D. Schuh, and M. Oestreich, Phys. Rev. Lett. **93**, 147405 (2004).
 - ¹⁷ L. Lombez, P. -F. Braun, H. Carrère, B. Urbaszek, P. Renucci, T. Amand, X. Marie, J. C. Harmand, and V. K. Kalevich, Appl. Phys. Lett. **87**, 252115 (2005).
 - ¹⁸ J. Strand, X. Lou, C. Adelmann, B. D. Schultz, A. F. Isakovic, C. J. Palmstrøm, and P. A. Crowell, Phys. Rev. B **72**, 155308 (2005).
 - ¹⁹ A. M. Tyryshkin, S. A. Lyon, W. Jantsch, and F. Schäffler, Phys. Rev. Lett. **94**, 126802 (2005).
 - ²⁰ A. W. Holleitner, V. Sih, R. C. Myers, A. C. Gossard, and D. D. Awschalom, cond-mat/0602155.
 - ²¹ M. I. D'yakonov and V. I. Perel', Zh. Éksp. Teor. Fiz. **60** 1954 (1971). [Sov. Phys. JEPT **33**, 1053 (1971)].
 - ²² G. Dresselhaus, Phys. Rev. **100**, 580 (1955).
 - ²³ Y. A. Bychkov and E. I. Rashba, Pis'ma Zh. Éksp. Teor. Fiz. **39**, 66 (1984) [Sov. Phys. JEPT Lett. **39** 78 (1984)].
 - ²⁴ D'yakonov and Kachorovskii, Fiz. Tekh. Poluprovodn. v 20, p 178 (1986) [Sov. Phys. Semicond. **20**, 110 (1986)].
 - ²⁵ X. Cartorixà, L. -W. Wang, D. Z. -Y. Ting, Y. -C. Chang, Phys. Rev. B **73**, 205341 (2006).
 - ²⁶ W. H. Lau and M. E. Flatté, Phys. Rev. B **72**, 161311(R) (2005).
 - ²⁷ J. Kainz, U. Rössler, and R. Winkler, Phys. Rev. B **70**, 195322 (2004).
 - ²⁸ W. H. Lau, J. T. Olesberg, and M. E. Flatté, Phys. Rev. B **64**, 161301(R) (2001); P. H. Song and K. W. Kim, Phys. Rev. B **66**, 035207 (2002); F. X. Bronold, I. Martin, A. Saxena, and D. L. Smith, Phys. Rev. B **66**, 233206 (2002); N. S. Averkiev, L. E. Golub, and M. Willander, J. Phys.: Condens. Matter **14**, R271 (2002); S. Krishnamurthy, M. van Schilfgaarde, and N. Newman, Appl. Phys. Lett. **83**, 1761 (2003); F. X. Bronold, A. Saxena, and D. L. Smith, Phys. Rev. B **70**, 245210 (2004); S. W. Chang and S. L. Chuang, Phys. Rev. B **72**, 115429 (2005); Z. G. Yu, S. Krishnamurthy, M. van Schilfgaarde, and N. Newman, Phys. Rev. B **71**, 245312 (2005); O. Bleibaum, Phys. Rev. B **69**, 205202 (2004); **71**, 235318 (2005); X. Cartoixà, D. Z. Y. Ting, and Y. C. Chang, Phys. Rev. B **71**, 045313 (2005).
 - ²⁹ M. W. Wu and H. Metiu, Phys. Rev. B **61**, 2945 (2000); M. W. Wu, J. Supercond. **14**, 245 (2001).
 - ³⁰ M. W. Wu and C. Z. Ning, Eur. Phys. J. B **18**, 373 (2000).
 - ³¹ M. W. Wu, J. Phys. Soc. Jpn. **70**, 2195 (2001).
 - ³² M. W. Wu and C. Z. Ning, Phys. Stat. Sol.(b) **222**, 523 (2000); M. W. Wu and M. Kuwata-Gonokami, Solid State Commun. **121**, 509 (2002).
 - ³³ J. L. Cheng, M. Q. Weng, and M. W. Wu, Solid State Commun. **128**, 365 (2003).
 - ³⁴ M. Q. Weng and M. W. Wu, Phys. Rev. B **66**, 235109 (2002); J. Appl. Phys. **93**, 410 (2003); M. Q. Weng, M. W. Wu, and Q. W. Shi, Phys. Rev. B **69**, 125310 (2004); L. Jiang, M. Q. Weng, M. W. Wu, and J. L. Cheng, J. Appl. Phys. **98**, 113702 (2005).
 - ³⁵ M. Q. Weng and M. W. Wu, Phys. Rev. B **68**, 075312 (2003); **71**, 199902(E) (2005); Chin. Phys. Lett. **22**, 671 (2005).
 - ³⁶ M. Q. Weng, M. W. Wu, and L. Jiang, Phys. Rev. B **69**, 245320 (2004).
 - ³⁷ M. Q. Weng and M. W. Wu, Phys. Rev. B **70**, 195318 (2004).
 - ³⁸ L. Jiang and M. W. Wu, Phys. Rev. B **72**, 033311 (2005).
 - ³⁹ C. Lü, J. L. Cheng, and M. W. Wu, Phys. Rev. B **73**, 125314 (2006).
 - ⁴⁰ J. L. Cheng and M. W. Wu, J. Appl. Phys. **99**, 083704 (2006).
 - ⁴¹ E. Ya. Sherman, Appl. Phys. Lett. **82**, 209 (2003).
 - ⁴² H. Haug and A. P. Jauho, *Quantum Kinetics in Transport and Optics of Semiconductor* (Springer-Verlag, Berlin, 1996).
 - ⁴³ P. Vogl, in *Physics of Nonlinear Transport in Semiconductor*, edited by K. Ferry, J. R. Barker, and C. Jacoboni (Plenum, New York, 1980).
 - ⁴⁴ G. D. Mahan, in *Polarons in Ionic Crystals and Polar Semiconductor*, edited by J. T. Devreese (North-Holland, Amsterdam, 1972).
 - ⁴⁵ *Semiconductors*, Landolt-Börnstein, New Series, Vol. 17a, ed. by O. Madelung (Springer, Berlin, 1987).
 - ⁴⁶ It is noted that the random phase approximation is valid for all the electron densities we discuss in the present paper according to the criterion given by M. Jonson, J. Phys. C **9**, 3055 (1976).
 - ⁴⁷ H. Haug and S. W. Koch, *Quantum theory of the optical and electronic properties of semiconductors* (World Scientific, Singapore, 2004).
 - ⁴⁸ *Semiconductors—Basic Data*, edited by Otfried Madelung (Springer, Berlin, 1996), p.p. 151; E. T. Yu, J. O. McCaldin, and T. C. McGill, Solid State Phys. **46**, 1 (1992).
 - ⁴⁹ X. L. Lei, J. L. Birman, and C. S. Ting, J. Appl. Phys. **58**, 2270 (1985).
 - ⁵⁰ M. Lundstrom, *Fundamentals of the Carrier Transport* (Cambridge University Press, Cambridge, England, 2000); J. Singh, *Physics of the Semiconductors and Their Heterostructures* (McGraw-Hill, New York, 1993).
 - ⁵¹ A. G. Aronov, G. E. Pikus, and A. N. Titkov, Zh. Éksp. Teor. Fiz. **84**, 1170 (1983) [Sov. Phys. JETP **57**, 680 (1983)].
 - ⁵² V. A. Marushchak, M. N. Stepanova, and A. N. Tikov, Fiz. Tverd. (Donetsk) **25**, 3537 (1983).
 - ⁵³ B. Jusserand, D. Richards, G. Allen, C. Priester, and B. Etienne, Phys. Rev. B **51**, 4707 (1994).
 - ⁵⁴ A. T. Gorelenko, B. A. Marushchak, and A. N. Tikov, Izv. Akad. Nauk SSSR, Ser. Fiz. **50**, 290 (1986).
 - ⁵⁵ M. Cardona, N. E. Christensen, and G. Fasol, Phys. Rev.

- B **38**, 1806 (1987).
- ⁵⁶ A. N. Chantis, M. van Schilfgaarde, and T. Kotani, Phys. Rev. Lett. **96**, 086405 (2006).
- ⁵⁷ It is difficult to give an exact analytical expression of τ_p^{ee} as we take into account of the Coulomb scattering to all orders as well as the counter effect of the Coulomb scattering to the inhomogeneous broadening. However, one can roughly estimate τ_p^{ee} by considering the Coulomb scattering to the lowest order (2nd order) and further ignoring the counter effect in the degenerate and non-degenerate limits following the approach in Ref. 59.
- ⁵⁸ P. Y. Yu and M. Cardona, *Fundamentals of Semiconductors* (Springer, Berlin, 2003), 3rd Ed., p. 222.
- ⁵⁹ M. M. Glazov and E. L. Ivchenko, Zh. Éksp. Teor. Fiz. **126** 1465 (2004) [JETP **99**, 1279 (2004)].
- ⁶⁰ M. M. Glazov and E. L. Ivchenko, Pis'ma Zh. Éksp. Teor. Fiz. **75**, 476 (2002) [JETP Lett. **75**, 403 (2002)].
- ⁶¹ In the weak scattering regime, the Coulomb scattering can also reduce the spin R/D time.³⁹
- ⁶² Private communication with R. T. Harley.
- ⁶³ It is stressed here that unlike the high temperature case where the preparation of the steady-state initial electron distributions under strong electric field proposed in Ref. 36 is not essential as the time scale to reach the steady state after turning on the electric field is negligible in comparison with the time scale of the spin R/D, at low temperature case due to the weak electron-AC phonon scattering, the preparation is essential as both time scales can be comparable to each other.
- ⁶⁴ A. P. Dmitriev, V. Yu Kachorovskii, M. S. Shur, and M. Strosio, Solid State Commun. **113**, 565 (2000); A. P. Dmitriev, V. Yu Kachorovskii, and M. S. Shur, J. Appl. Phys. **89**, 3793 (2001).
- ⁶⁵ E. M. Conwell, *High Field Transport in Semiconductors* (Academic press, New York and London, 1967), p. 21.